

A parameter-free statistical model for two-dimensional carbon nanostructures

Chang-Chun He,^{1, a)} Shao-Gang Xu,^{2, 3, a)} Jiarui Zeng,¹ Weijie Huang,¹ Yao Yao,^{1, 4} Yu-Jun Zhao,¹ Hu Xu,^{2, 3, b)} and Xiao-Bao Yang^{1, c)}

¹⁾*School of Physics and Optoelectronics, South China University of Technology, Guangzhou 510640, China*

²⁾*Department of Physics, Southern University of Science and Technology, Shenzhen 518055, China*

³⁾*Quantum Science Center of Guangdong-Hong Kong-Macao Greater Bay Area (Guangdong), Shenzhen 518045, People's Republic of China*

⁴⁾*State Key Laboratory of Luminescent Materials and Devices, South China University of Technology, Guangzhou 510640, China*

(Dated: 19 December 2024)

Energy degeneracy in physical systems may be induced by symmetries of the Hamiltonian, and the resonance of degeneracy states in carbon nanostructures can effectively enhance the stability of the system. Combining the octet rule, we introduce a parameter-free statistical model to determine the physical properties by lifting the energy degeneracy in carbon nanostructures. This model offers a direct path to accurately ascertain electron density distributions in quantum systems, akin to how charge density is used in density functional theory to deduce system properties. Our methodology diverges from traditional quantum mechanics, focusing instead on this unique statistical model by minimizing bonding free energy to determine the fundamental properties of materials. Applied to carbon nanoclusters and graphynes, our model not only precisely predicts bonding energies and electron density without relying on external parameters, but also enhances the prediction of electronic structures through bond occupancy numbers, which act as effective hopping integrals. This innovation offers insights into the structural properties and quantum behavior of electrons across various dimensions.

I. INTRODUCTION

Energy degeneracy resulting from latent symmetry is a crucial aspect of quantum systems, contributing to various quantum phenomena^{1–3}. The latent symmetry is attributed to the symmetry of the isospectral effective Hamiltonian obtained through subsystem partitioning, and the rotational symmetries can be broken in a controlled manner while maintaining the more fundamental symmetry⁴. Lifting the degeneracy by external perturbations can lead to a lower energy state with energy level splitting. For instance, the Jahn-Teller effect describes how local geometric distortions can lower the overall energy of a system by removing degeneracy⁵. In carbon nanostructures, quantum resonance provides another mechanism for lifting energy degeneracy by the combination of possible degenerate Kekulé structures, emerging delocalized electron states and aromaticity to further stabilize the system^{6–8}. For the benzene molecule, there are two Kekulé structures with C_3 symmetry that both meet the octet rule, exhibiting the two-fold energy degeneracy. Resonance theory shows that the uniform superposition of Kekulé structures with C_6 symmetry corresponds to the true electron density of benzene⁹, lifting the energy degeneracy with additional resonance energy.

Generally, a polycyclic aromatic hydrocarbon (PAH) molecule has a series of Kekulé structures that satisfy

the octet rule in degenerate energy state. To construct the most valuable one to represent all Kekulé structures, Clar's rule identifies the key structure by maximizing the number of nonadjacent π -sextets¹⁰. The nonadjacent π -sextets have two forms with alternating single and double bonds, independently contributing a statistical weight of 2, and the statistical weight is 2^N for N π -sextets. Therefore, Clar's rule provides an avenue to lift energy degeneracy by favoring the structure with the largest statistical weight, which best approximates the relative stability of various carbon nanostructures^{11–14}. The sextets predicted by Clar's rule generally correspond to aromatic rings, aligning with various theoretical methods^{15,16}, though exceptions exist in irregular-shaped PAHs¹⁷. Additionally, PAH isomers with more sextets tend to exhibit higher kinetic stability, lower reactivity, and larger energy gaps¹⁸. Despite the success in interpreting chemical bonding, the empirical rules limit quantitative electron distribution analysis for lack of rigorous mathematical foundation in quantum theory^{19–21}. A single Clar structure often cannot accurately reproduce the actual electron density distribution of a PAH molecule, as the symmetry of the Clar structure often disagrees with the realistic molecular symmetry²².

The Clar's rule, as a parameter-free model, falls short in accurately predicting the electron density along with structural stabilities and electronic properties of carbon nanostructures. Current quantitative models require training data from DFT to acquire model parameters and precisely predict the properties of unknown structures, which belong to a first-principles-based (second-principles) scheme²³. To address electronic properties,

^{a)}These authors contributed equally.

^{b)}Electronic mail: xuh@sustech.edu.cn

^{c)}Electronic mail: scxbyangscut@scut.edu.cn

the tight-binding (TB) model offers a simpler method to construct an effective Hamiltonian²⁴, but it relies on DFT or experimental data for integral parameters²⁵. Several deep learning methods have been proposed to predict structural properties after fitting millions of parameters based on massive data from DFT^{26–28}. However, the inherent chemical origin and deeper insights into specific systems are obscured by the intricate neural network model. Therefore, there is a need for a more direct parameter-free method that can both conceptualize and quantify the electron density distribution, providing a deeper understanding of chemical bonding in carbon nanostructures.

In this work, we introduce a streamlined parameter-free statistical bonding free energy (BFE) model for determining electron density distribution by lifting the energy level in carbon nanostructures. The predicted structural properties of this model remarkably align with both experimental findings and first-principles calculations. By integrating the octet rule with the BFE model within a grand canonical ensemble, we can accurately evaluate bonding energies, uncovering significant contributions of bonding entropy to structural stability in carbon nanostructures. Furthermore, the occupancy numbers (ONs) of each C-C bond derived from our model predict the electron density and bond length. These ONs can serve as hopping integrals in the TB models, thereby simplifying accurate predictions of electronic structures, including energy gaps, energy levels, and the corresponding spatial distribution of wavefunctions. Local aromaticity is defined by the mean value of ONs in each six-membered ring, offering a simple yet effective method to measure electron delocalization in the π -conjugated system. Our method provides valuable insights into the structural properties and quantum behavior of electrons across different dimensional carbon nanostructures.

II. RESULTS AND DISCUSSION

A. The derivation of bonding free energy model

To understand the interatomic interactions in carbon nanostructures, we start from the simple benzene molecule, which has two different forms of alternating single and double bonds that obey the octet rule as shown in the top panel of FIG. 1(a). The degenerated Kekulé structures hold three-fold symmetry, where the fictional C-C double bond is stronger than C-C single bond, violating the identical C-C bonds in the benzene molecule. To lift the two-fold degenerate energy level, the equally weighted superposition of two Kekulé structures can satisfy the intrinsic symmetry as depicted in the middle panel of FIG. 1(a), which has the lowest energy due to the additional resonance energy. From the view of molecular theory, the optimal state ψ_1 is the resonance of two equal Kekulé structures, thus the resonance weight is $1/\sqrt{2}$ to ensure that the ONs of all C-C bonds are identical to 1.5,

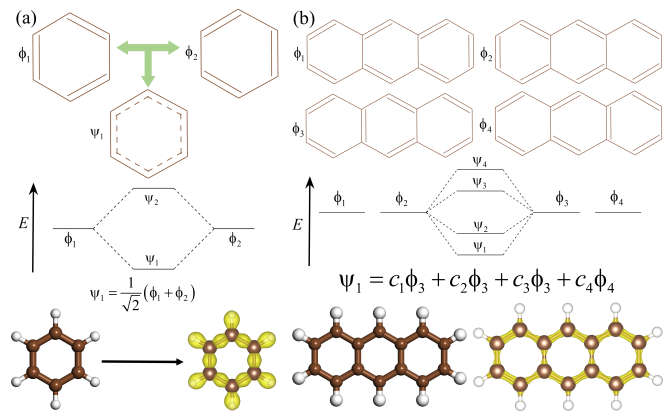


FIG. 1. (a) Top part is two Kekulé structures (denoted by ϕ_1, ϕ_2) and the average structure of benzene (denoted by ψ_1); middle part is the energy level diagram of two degenerate state ϕ_1, ϕ_2 ; bottom part is the structure and charge distribution of benzene calculated by DFT. (b) Top part is four Kekulé structures of anthracene (denoted by $\phi_1-\phi_4$); middle part is the energy level diagram of four degenerate state $\phi_1-\phi_4$ with the undetermined parameters; bottom part is the structure and charge density of anthracene calculated by DFT.

in agreement with the charge density distribution derived from DFT as shown in bottom part of FIG. 1(a). For any carbon nanostructures, the ground state can be represented by the linear combinations of a series of degenerate Kekulé structures²⁹, but the resonance weights can not directly derived unless from first-principles calculations. For instance, the anthracene has four Kekulé structures (see FIG. 1(b)). Particularly, the charge density from DFT shows that the edge C-C bonds are stronger than the inner C-C bonds in the bottom part of FIG. 1(b), but we can not determine the accurate ONs of C-C bond, while the proposed BFE model can easily calculate the resonance weights with external parameters.

For a given carbon nanostructure, a series of possible degenerate Kekulé structures satisfy the octet rule. Assuming that all electrons are mobile across all chemical bonds and the number of electrons in each bond is variable, the system can be considered as a grand canonical ensemble. In this framework, the total electrons in the system are allocated across each bond as demonstrated in FIG. 2(a), where each bond contains n_i electrons, associated with a chemical potential μ_i , and upholds the total electron constraint $\sum_{i=1}^{N_{\text{bond}}} n_i = N_{\text{ele}}$. Here, N_{bond} and N_{ele} denote the total numbers of bonds and electrons, respectively. Assuming that the internal energy for C-C bonds is equivalent, the chemical potential μ_i can be used to distinguish nonequivalent C-C bonds, with internal energy U set to zero for simplicity. The grand canonical partition function is derived by

$$\mathcal{Z} = \sum_{n_1, \dots, n_{N_{\text{bond}}}} e^{-\sum_{i=1}^{N_{\text{bond}}} (n_i \alpha_i + U)} = \left(\sum_{i=1}^{N_{\text{bond}}} e^{-\alpha_i} \right)^{N_{\text{ele}}}, \quad (1)$$

where $\alpha_i = -\frac{\mu_i}{k_B T}$ is the reduced chemical potential. The

first equality encompasses the ergodic combinations of electron numbers for each bond^{30,31}, including all possible Kekulé structures. The second equality holds because all combinations correspond to a multinomial expansion, where the multinomial coefficients correspond to the multiplicity of each combination. We then express the formula for free energy as:

$$F = N_{\text{ele}} k_B T \sum_{i=1}^{N_{\text{bond}}} p_i \log p_i = -N_{\text{ele}} k_B T S_b, \quad (2)$$

where the bonding entropy S_b is $-\sum_{i=1}^{N_{\text{bond}}} p_i \log p_i$. p_i is the electron probability in bond i , defined by

$$p_i = \frac{n_i}{N_{\text{ele}}} = -\frac{1}{N_{\text{ele}}} \frac{\partial F}{\partial \mu_i} = \frac{e^{-\alpha_i}}{\sum_{i=1}^{N_{\text{bond}}} e^{-\alpha_i}}. \quad (3)$$

It is significant to note that the energy is roughly proportional to the total number of electrons N_{ele} in the system, and the bonding entropy is proportional to $\log N_{\text{ele}}$. We introduce the concept of an equivalent ‘‘temperature’’ to redefine the bonding free energy:

$$F_b(p_1, \dots, p_{N_{\text{bond}}}) = \frac{N_{\text{ele}} k_B T_0}{\log N_{\text{ele}}} \sum_{i=1}^{N_{\text{bond}}} p_i \log(p_i), \quad (4)$$

where the equivalent ‘‘temperature’’ $k_B T$ is $\frac{k_B T_0}{\log N_{\text{ele}}}$, T_0 is the equivalent ‘‘standard temperature’’, and $k_B T$ functions as the coefficient to ensure that F_b is an extensive quantity as detailed in the Supplementary Material (SM). The F_b as a function of p_i is determined by Eq. 4, where the minimal F_b corresponding to the maximum bonding entropy S_b can decide the ground state electron density for carbon nanostructures. Here, we take anthracene as an example to show how to determine the p_i of each bond. The variation of F_b with ϕ_1 and ϕ_2 is given in FIG. 2(b), where the global minimum ϕ_0 without any constraints is marked by the orange pentagon. ϕ_0 represents the equal electron probability for each bond, which contradicts the actual electron distribution of the molecule due to varying bonding environments for each carbon atom.

The identification of the minimal F_b is essential, particularly under local bonding constraints ensuring each carbon atom adheres to the octet rule^{32,33}. For instance, we apply the constraint $n_1 + n_2 = 6$ to carbon atom 1, taking into account the two-electron requirement of the C-H bond to satisfy the duplet rule for hydrogen. FIG. 1(c) shows four Kekulé structures that satisfy the octet rule, with their respective F_b values depicted in FIG. 2(b). The pink line represents the area compliant with the octet rule in FIG. 1(b), and the red pentagon indicates the optimal electron density of ϕ_* as depicted in FIG. 2(c). The F_b for ϕ_* distribution is notably lower than that of the Kekulé structures, indicating greater stability in the resonance structure compared to a single Lewis structure. Similar to bond order, the ONs of

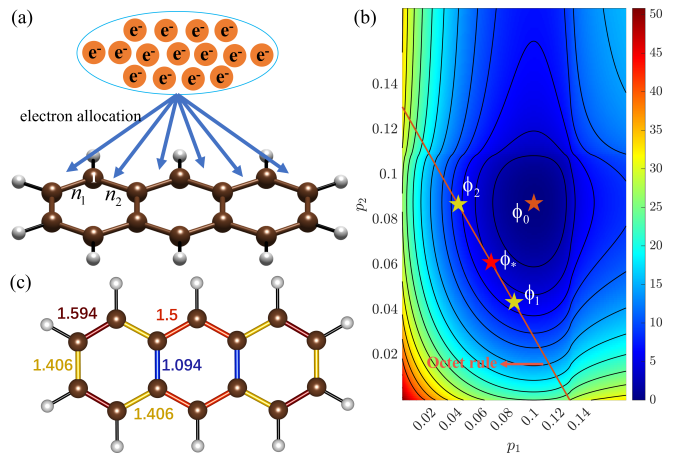


FIG. 2. (a) Total electron allocation model for anthracene molecule. (b) The bonding free energy surface varied with p_1 and p_2 for anthracene molecule. (c) The optimal occupancy number of each bond for anthracene molecule, and the ON number is marked near the bond.

each bond, defined by $n_i/2$ for C-C bonds in two-center two-electron bonds, are indicated near each inequivalent bond. Note that the predicted ONs are in good agreement with the molecular symmetry compared with the Clar structure³⁴.

B. Energy prediction ability of BFE model

According to the BFE model, the bond energies of carbon nanostructures can be expressed by F_b . Thus, the relative stability of isomers can be distinguished by global minimum F_b . As reflected in FIG. 3(a), the first-principles calculations based on highly precise CCSD(T)/CBS method³⁵ proves that triphenylene with three-fold symmetry is the most stable among $C_{18}H_{12}$ molecules. Interestingly, the F_b of triphenylene is lower than that of chrysene, aligning well with the CCSD(T)/CBS method. Further, the F_b has well agreement with bonding energy calculated by DFT for the PAH structures comprising fewer than 30 carbon atoms, as shown in FIG. S1 of SM. Thus, BFE effectively describes PAH stability without external parameters, offering a distinct perspective on isomerization energies. As shown in the inset of FIG. 3(a), the ONs in these structures reflect the symmetry of the molecules and align with the charge density distribution obtained from DFT, implying that the ON can reflect the local electron distribution. Moreover, FIG. 3(b) reveals a strong linear relationship between the ON of bonds and bond length, where shorter bond lengths corresponding to higher ON values with stronger interactions. Triphenylene, which identified as the most stable molecule, has the lowest ON deviation from 1.5, whereas other molecules show significant deviations, contributing to their relative instability.

Having established the BFE model of PAH structures,

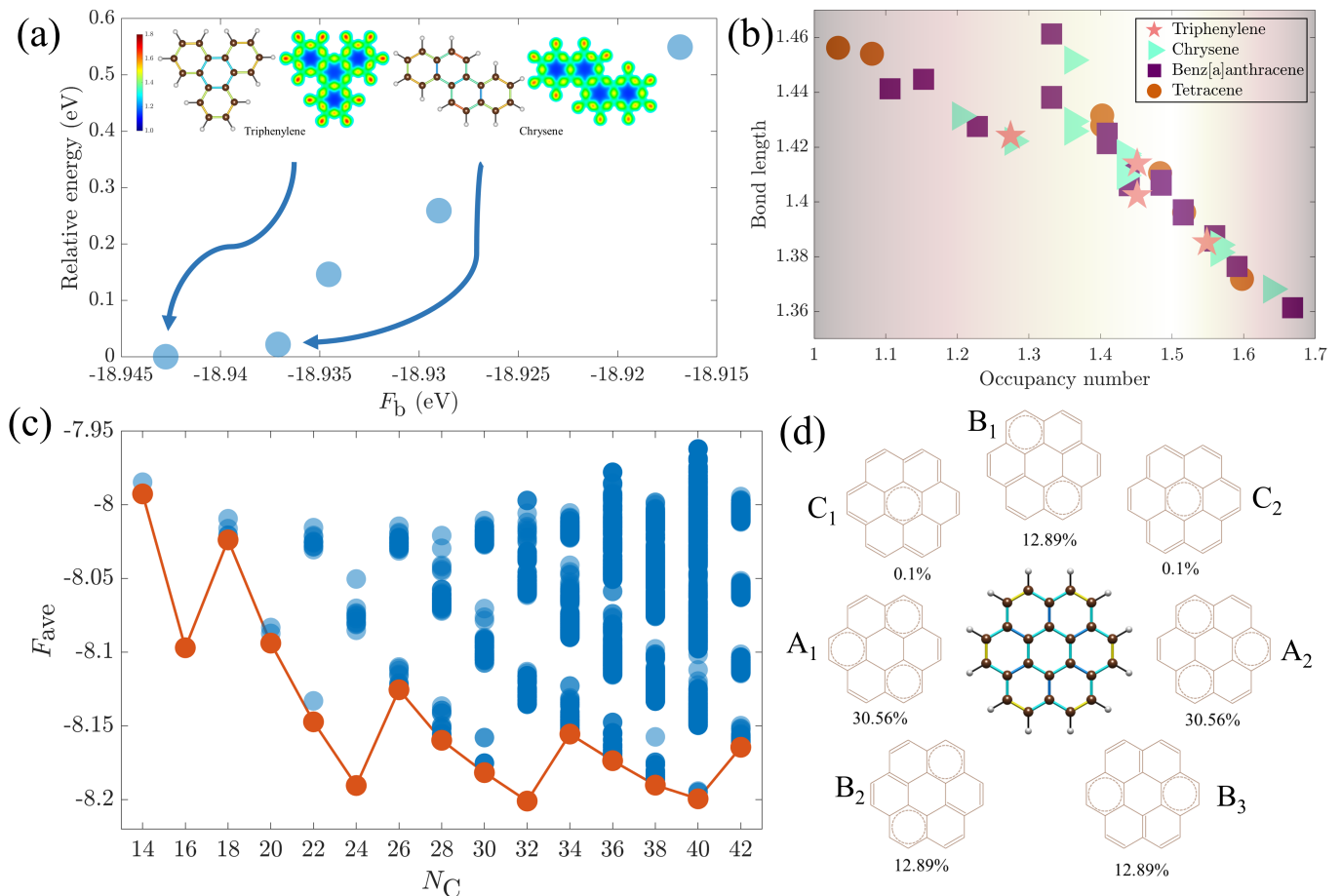


FIG. 3. (a) The linear relationship between the relative energy predicted by the DFT and F_b calculated by BFE model, where the charge density and ON of two stable $C_{18}H_{12}$ molecules are plotted in the inset. (b) The relationship between the ON predicted by BFE model and bond length determined by the DFT. (c) The convex-hull of F_{ave} predicted by BFE model, and the convex points are marked by pink circles. (d) The seven resonance structures for coronene molecule, and the derived resonance weights is marked near the structures.

we are able to predict stable magic PAH clusters using the average BFE, $F_{ave} = \frac{F_b}{N_C}$, where N_C is the total number of carbon atoms. As shown in FIG. 3(c), we generated all PAH structures comprising fewer than 42 carbon atoms. This allows us to investigate the variation of average BFE as a function of N_C and the corresponding magic structures. Notably, the trend of F_{ave} is the same as the formation energy derived from DFT calculations²⁵, where the identified magic clusters, including $C_{16}H_{10}$, $C_{24}H_{12}$, $C_{32}H_{14}$, and $C_{40}H_{16}$ are depicted in FIG. S2 of SM. Therefore, F_{ave} serves as a reliable metric for evaluating the structural stability and predicting the ground state structures, including the electron density distribution, which is equivalent to the DFT-based Hamiltonian.

Beyond the stability evaluation, the resonance weights W_R (satisfying $W_R > 0$, $\sum_R W_R = 1$) of all resonance structures can be defined by the optimal resonance-type representation of ϕ_* determined by the minimal BFE

model³⁶:

$$W_R = \operatorname{argmin} \|\phi_* - \sum_R W_R \phi_R\|, \quad (5)$$

where ϕ_R represents the ON of resonance structures (the C-C single bond is 1, the C-C double bond is 2, and C-C partial double bond is 1.5 like benzene), and the ϕ_* represents the ON of the structures derived by BFE model. The weights for anthracene in FIG. 1(b) are $c_1 = c_4 = 40.6\%$, $c_2 = c_3 = 9.4\%$. In addition, we take the coronene, as a magic cluster in FIG. 3(c), to show how to calculate the resonance weight, where the optimal electron distribution is shown in the center of FIG. 3(d). The seven surrounding structures are classified into three categories. The A_1 , A_2 , structures with three Clar rings in the left-center and right-center, as the most significant contributors, occupy the highest proportion of 61.12%. Next are three structures (B_1 , B_2 , B_3) with two Clar rings, which occupy about 38.67% contribution. Lastly, the two structures (C_1 , C_2) at the left-top and the right-top, each with only one Clar ring, contribute only

0.2%. The result also has good agreement with the previous work¹⁹ and Clar’s rule³⁴, where the more aromatic π -sextets will contribute higher stability.

To validate the generality of the BFE model, we also considered other carbon-rich clusters as shown in FIG. 4. These molecules were evaluated using DFT calculations^{37,38}, in which the stability of structures with low energy is confirmed by the high-level Heyd-Scuseria-Ernzerhof (HSE06) calculation^{39,40} as detailed in SM. We take $C_{96}H_{48}$ with 24 hexagonal rings as an example to demonstrate the predictive power in cycloarenes, which mainly consist of two types of structures: kekulene and clarene^{41,42}. FIG. 4(a) clearly shows that the BFE has good linear consistence with the relative energy from DFT calculations. The most stable structure is marked in the left-top part of FIG. 4(a), in which the hexagonal rings stack with staggered alignment rather than arranged in a single row, since the ON of each bonds is more uniform to gain more bonding entropy. In contrast, the structure of highest energy in the right-bottom of FIG. 4(a) is composed of three elongated PAH clusters, losing more bonding entropy. FIG. 4(b) shows that the carbon nanobelt, which are rigid and thick segments of carbon nanotubes⁴³, can also be accurately predicted. Similar to cycloarenes, the most stable carbon nanobelt has the hexagonal rings in a staggered arrangement, while the most unstable nanobelt also has elongated PAH clusters. Therefore, the elongated PAH clusters will remarkably contribute instability, which originates from the reactivate stability between anthracene and phenanthrene.

Next we focus on the carbon nanostructures with pentagon rings as shown in FIG. 4(c), in which the structure with isolated pentagons has the lowest energy as predicted by BFE model and DFT calculations. The isolated pentagons can lead to a more evenly distribution of ONs in the carbon nanostructure. The more adjacent pentagons there are, the less stable the structure becomes as depicted in FIG. 4(c). In addition to C-H systems, C-H-O systems can also be described by BFE model, where the most stable structure occurs when the two oxygen atoms are in the ortho-position as shown in FIG. 4(d). Because the C-O is a double bond, then the bond distribution will be completely different with the introduction of oxygen atoms. Note that the carbon atom connected to oxygen atom will bonded two other carbon atoms by single bond, the ortho-oxygen atoms will result in the entire system having only three C-C single bonds, thereby reducing one single bond, which effectively increases the bonding entropy and enhances the structural stability. Therefore, the BFE model can excellently predict the reactivate stability among widespread carbon nanostructures, which is compatible with previous theory.

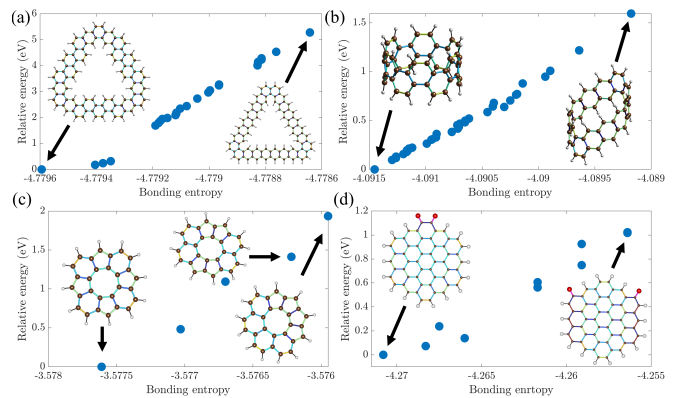


FIG. 4. The relationship between relative energy calculated by DFT and bonding entropy for (a) cycloarenes; (b) carbon nanobelt; (c) carbon nanostructures with pentagon rings; (d) C-H-O systems.

With a given carbon nanostructure, there are numerous combinations that meet the octet rule, and the charge density is attributed to all these combinations according to BFE model. The most likely electron distribution is deduced through ergodic theory, which entails averaging over all possible distributions⁴⁴. The minimal F_b thus determines the optimal electron distribution with the maximum bonding entropy for a system, suggesting a uniform electron density to maximize resonance energy. Viewed as preliminary information, the number of the total electron constraint and octet rule aptly reflect the most informed current understanding, in line with the principle of maximum entropy⁴⁵. Our BFE model emphasizes the important role of bonding entropy in the carbon nanostructures, where the stabilities are dominated by delocalized electrons.

C. Electron structures prediction capability of BFE model

Due to the outstanding optoelectronic properties and applications in organic field-effect transistors^{46–48}, the electronic structures of carbon nanostructures have attracted significant attention in both experimental and theoretical domains^{49,50}. The TB model is typically employed to describe the electronic structures, which often requires DFT calculations to fit integral parameters. Previous research indicates that accurately predicting energy gaps in PAHs requires up to thirteen hopping integral parameters²⁵, essential for differentiating various C-C bonds. Herein, we assume the hopping parameter is proportional to the ON of the bond between carbon atoms i and j , constructing the TB Hamiltonian for PAHs with nearest-neighbor couplings as follows:

$$H = - \sum_{i,j} t_{i,j} (c_i^\dagger c_j + h.c.) \quad (6)$$

where the on-site energy is set to zero, $t_{i,j}$ is the hopping integral, the subscript i, j represents the indices of the

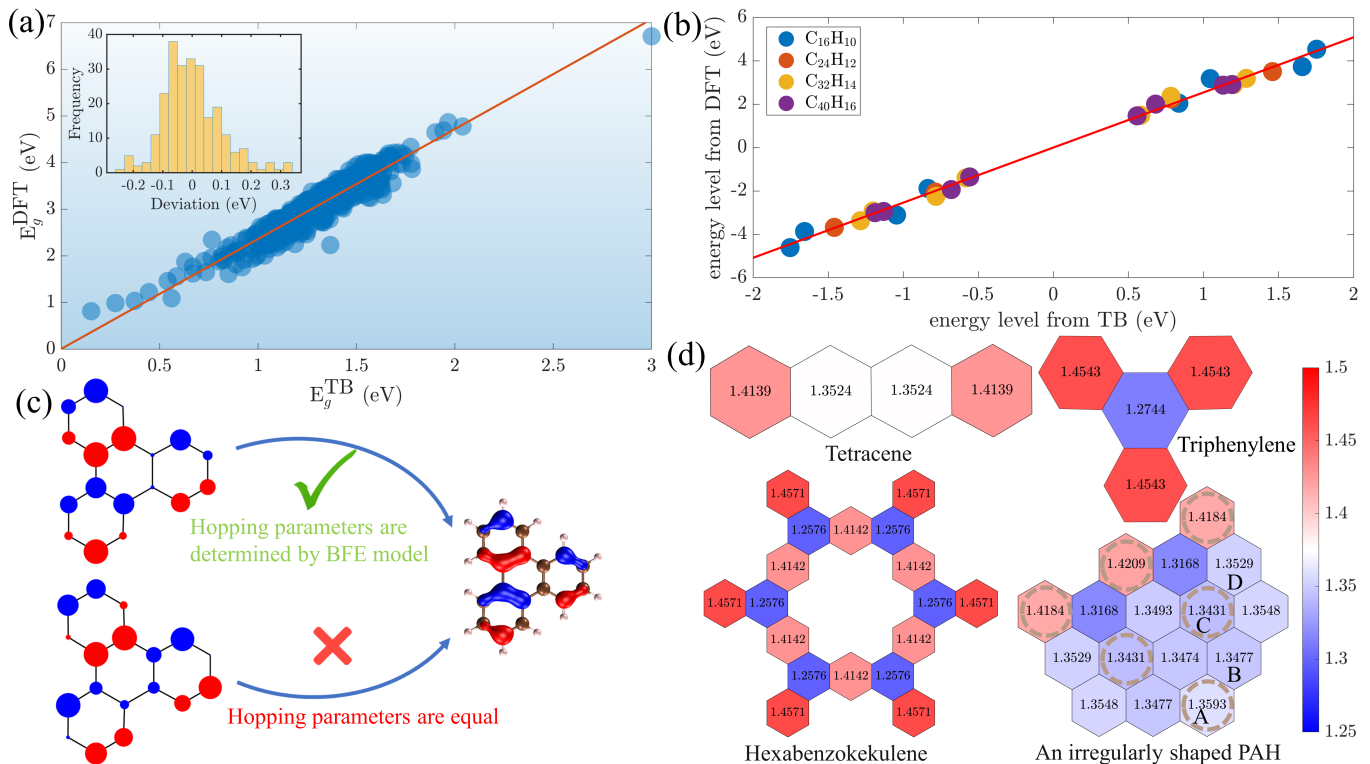


FIG. 5. (a) The linear relationship between the energy gaps predicted by the TB method and those calculated by DFT, with the deviation distribution plotted in the inset. (b) The excellent agreement between energy level predicted by TB model and DFT. (c) The molecular orbitals determined by the TB model (left panel) and DFT (right panel). (d) The defined local aromaticity for three representative molecules, where the color corresponds to the right colorbar.

nearest neighboring carbon atoms, and c_i^\dagger , c_j are the creation and annihilation operators of the π electron at sites i and j , respectively. The predicted energy gap by the TB model shows a linear correlation with the DFT-calculated energy gap in the HSE06 level, as depicted in FIG. 3(a). This relationship is expressed as $E_g^{\text{DFT}} = \gamma \times E_g^{\text{TB}} + E_g^0$, with parameters $\gamma = 2.355$ and $E_g^0 = 0.01$ eV. Notably, over 70% of the energy gaps predicted by the TB model deviate less than 0.1 eV from those of the DFT calculations as shown in the inset of FIG. 5(a), using only two external parameters, namely γ and E_g^0 . This underscores the efficacy of the ON in reflecting the hopping integral and bond strength. Additionally, the energy levels of the magic PAH clusters are also accurately predicted, as plotted in FIG. 5(b). Therefore, the ON of bonds serves as a reliable descriptor for predicting the electronic structures of PAHs, effectively capturing both structural stability and charge density.

To investigate the wavefunction of molecular orbitals, we choose the highest occupied molecular orbital (HOMO) of triphenylene molecule to demonstrate the accuracy of our TB model. The coefficients of each atomic orbitals are the eigenvectors corresponding to the HOMO energy level as shown in the upper left corner of FIG. 5(c), where the radius of the circles represents the magnitude of the coefficients. Note that red represents posi-

tive values while blue represents negative values, which is consistent with the spatial distribution of wavefunctions calculated by DFT, as shown in the right panel of FIG. 5(c). As a comparison, the bottom left part of FIG. 5(c) shows the calculated molecular orbitals when all hopping integrals between the nearest neighbors are equal. Unfortunately, the magnitude of coefficients on each C atom does not correspond to the calculations by DFT in the right panel of FIG. 5(c), highlighting the importance of distinguishing C-C bonds. It is noteworthy that both the HOMO and the lowest unoccupied molecular orbital (LUMO) are two-fold degenerate, where the four molecular orbitals are detailed in the SM.

As shown in FIG. 5(d), tetracene with a linear arrangement of acenes is less stable than triphenylene with Y-type acenes, and the energy gap of tetracene is smaller than that of triphenylene¹⁸. Here we define the mean value κ of ONs on six-membered rings to describe the local aromaticity. We can assert that the ring is akin to the “fully-aromatic” benzene if κ approaches 1.5; otherwise, it exhibits less aromaticity. It is apparent that κ values in triphenylene are larger than those in tetracene, which suggests additional aromaticity and stability¹³. The defined κ offers an avenue to describe the aromaticity, providing insight into the electronic properties of PAHs. Furthermore, triphenylene can self-assemble into a hexabenzokekulene with six-fold symmetry⁵¹, which has the

largest energy gap among all isomers. Note that the hexabenzozekulene holds 12 highly aromatic rings with red coloring of the 18 hexagonal rings, in which a particularly high proportion of aromatic rings results in a larger band gap and high stability. FIG. 5(d) shows the large irregularly shaped PAHs as the Clar’s rule-breaking examples¹⁷, where the Clar’s rule shows that the A, C rings are more aromatic than ring B, D. However, according to several aromaticity descriptors on the rings (MCI^{1/n}, HOMA, and NICS(1)_{zz}), the aromaticity of ring A-D is comparable¹⁹, which is also in good agreement with the local aromaticity description in our parameter-free model.

For sp^2 bonded carbon nanoclusters with 2c-2e bonds, the combined use of the BFE and the octet rule has been effective in predicting various properties. We have extended this approach to sp - sp^2 hybridized graphyne structures^{52,53}, showing the capability of BFE in forecasting structural properties in periodic systems. Unlike isolated PAH structures, periodic boundary conditions needs to be considered in the unit cell for graphyne. We have systematically generated a range of nonequivalent candidates for sp - sp^2 hybridized carbon allotropes, covering numbers of carbon atoms from 12 to 60⁵⁴. The definition of BFE for graphyne follows Eq. 4, where the globally minimal BFE corresponds to the bonding energy. Consequently, the BFE can elucidate structural stability in both molecular and periodic systems, highlighting its wide-ranging applicability.

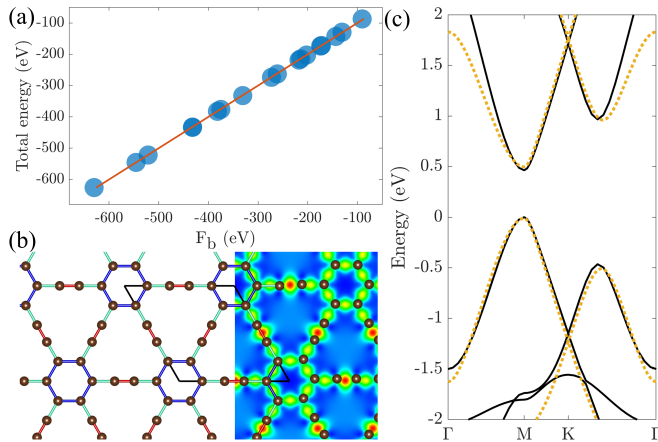


FIG. 6. (a) The linear correlation between BFE and bonding energy derived from DFT. (b) Distribution of ON and charge density for the γ -graphyne structure. (c) The band structure determined by the DFT method (solid line) and the TB method (dashed line).

Moving beyond structural stability, we focus on the electronic structures of graphynes. For the synthesized γ -graphyne⁵⁵, we present the predicted ON of each bond alongside the charge density in Fig. 6(b). It is observed that bonds between two-coordinate carbon atoms are stronger than those between three-coordinate carbon atoms, as indicated by the higher ON and the red

area in the charge density distribution. By optimizing ON of each bond to minimize BFE, we construct a TB model for graphyne, contributed by p_z electrons, to analyze electronic structures. In this model, the hopping integral is proportional to the exponential of the ON. The TB-based band structures (dashed line) as given in Fig 6(c), which show considerable agreement with DFT results (solid line) near the Fermi level. A single proportionality coefficient is fine-tuned to match the band gap determined by DFT. This matching process underscores the effectiveness of ON in differentiating hopping integrals between nearest carbon atoms. The band structure predictions for other graphyne structures are further detailed in FIG. S4 of SM. Here, the optimal ON for each bond serves as a reliable measure of the bond strength and effectively describes the electronic structures of various dimensional systems.

III. CONCLUSIONS

In conclusion, for the first time, we have developed a parameter-free statistical model that determines the electron density and related properties in carbon nanostructures across various dimensions. Without relying on pre-training data from DFT, the bonding free energy defined in our model shows a linear correlation with the bonding energy derived from DFT. This highlights the crucial role of bonding entropy in stabilizing carbon nanostructures with delocalized electrons. The optimal occupancy number of each bond accurately reflects bond strength and closely correlates with bond length and charge density distribution, which also serves as the basis for determining hopping integrals when constructing TB models. These TB models have proven effective in predicting electronic structures for various dimensional carbon nanostructures, thus enriching our understanding of electronic behaviors. Furthermore, the mean value of the occupancy number offers a measure of local aromaticity for six-membered rings, aligning well with current calculations for aromaticity. By incorporating bonding free energy, we provide a statistical perspective to understand the quantum behaviors of electrons, offering a concise yet precise approach for determining structural stability and electronic properties in carbon nanoclusters and graphynes, which may also hold potential for broad applicability in other systems as well.

IV. SUPPLEMENTARY MATERIAL

The supplementary material contains information of the computational methods, the detailed derivation of bonding free energy model, the energy level and aromaticity prediction of PAH molecules and the band structure prediction of graphynes.

V. AUTHOR DECLARATIONS

Conflict of Interest

The authors have no conflicts to disclose.

ACKNOWLEDGMENTS

This work is supported by Guangdong Basic and Applied Basic Research Foundation (Grant No. 2023A1515110894 and No.2023A1515010734), Guangdong Provincial Key Laboratory of Functional and Intelligent Hybrid Materials and Devices (Grant No. 2023-GDKLFIHMD-04), the National Natural Science Foundation of China (Grant No. 12374182 and No. 12204224) and the Shenzhen Science and Technology Program (Grant No. RCYX20200714114523069).

- ¹B. T. Matthias, T. H. Geballe, and V. B. Compton, Superconductivity, *Rev. Mod. Phys.* **35**, 1 (1963).
- ²K. von Klitzing, Quantum hall effect: Discovery and application, *Annual Review of Condensed Matter Physics* **8**, 13 (2017).
- ³R. Tsu and L. Esaki, Tunneling in a finite superlattice, *Appl. Phys. Lett.* **22**, 562 (1973).
- ⁴M. Röntgen, M. Pyzh, C. V. Morfonios, N. E. Palaiodimopoulos, F. K. Diakonou, and P. Schmelcher, Latent symmetry induced degeneracies, *Phys. Rev. Lett.* **126**, 180601 (2021).
- ⁵H. A. Jahn, E. Teller, and F. G. Donnan, Stability of polyatomic molecules in degenerate electronic states - i—orbital degeneracy, *Proc. R. Soc. London A: Math. Phys. Sci.* **161**, 220 (1937).
- ⁶P. Muller, Glossary of terms used in physical organic chemistry (iupac recommendations 1994), *Pure Appl. Chem.* **66**, 1077 (1994).
- ⁷A. Narita, X.-Y. Wang, X. Feng, and K. Müllen, New advances in nanographene chemistry, *Chem. Soc. Rev.* **44**, 6616 (2015).
- ⁸X.-Y. Wang, A. Narita, and K. Müllen, Precision synthesis versus bulk-scale fabrication of graphenes, *Nat. Rev. Chem.* **2**, 0100 (2017).
- ⁹Y. Liu, P. Kilby, T. J. Frankcombe, and T. W. Schmidt, The electronic structure of benzene from a tiling of the correlated 126-dimensional wavefunction, *Nat. Commun* **11**, 1210 (2020).
- ¹⁰E. Clar, The aromatic sextet, in *Mobile Source Emissions Including Polycyclic Organic Species*, edited by D. Rondia, M. Cooke, and R. K. Haroz (Springer Netherlands, Dordrecht, 1983) pp. 49–58.
- ¹¹Y.-W. Son, M. L. Cohen, and S. G. Louie, Energy gaps in graphene nanoribbons, *Phys. Rev. Lett.* **97**, 216803 (2006).
- ¹²T. Cao, F. Zhao, and S. G. Louie, Topological phases in graphene nanoribbons: Junction states, spin centers, and quantum spin chains, *Phys. Rev. Lett.* **119**, 076401 (2017).
- ¹³M. Randić, Aromaticity of polycyclic conjugated hydrocarbons, *Chem. Rev.* **103**, 3449 (2003).
- ¹⁴T. Wassmann, A. P. Seitsonen, A. M. Saitta, M. Lazzeri, and F. Mauri, Clar’s theory, π -electron distribution, and geometry of graphene nanoribbons, *J. Am. Chem. Soc.* **132**, 3440 (2010).
- ¹⁵M. Randić and A. T. Balaban, Partitioning of π -electrons in rings for clar structures of benzenoid hydrocarbons, *J. Chem. Inf. Model.* **46**, 57 (2006).
- ¹⁶Y. Ruiz-Morales, The agreement between clar structures and nucleus-independent chemical shift values in pericondensed benzenoid polycyclic aromatic hydrocarbons: an application of the y-rule, *J. Phys. Chem. A* **108**, 10873 (2004).
- ¹⁷N. Nishina, M. Makino, and J.-i. Aihara, Aromatic character of irregular-shaped nanographenes, *J. Phys. Chem. A* **120**, 2431 (2016).
- ¹⁸K. Strutynski, A. Mateo-Alonso, and M. Melle-Franco, Clar rules the electronic properties of 2d π -conjugated frameworks: Mind the gap, *Chem. Eur. J.* **26**, 6569 (2020).
- ¹⁹Y. Wang, Quantitative resonance theory based on the clar sextet model, *J. Phys. Chem. A* **126**, 164 (2022).
- ²⁰Y. Wang, Extension and quantification of the fries rule and its connection to aromaticity: Large-scale validation by wavefunction-based resonance analysis, *J. Chem. Inf. Model.* **62**, 5136 (2022).
- ²¹I. Gutman, S. Radenkovic, M. Antic, and J. DJurdjevic, A test of clar aromatic sextet theory, *J. Serb. Chem. Soc.* **78**, 1539 (2013).
- ²²S. Cyvin and I. Gutman, Kekulé structures and their symmetry properties, *Comput. Math. Appl.* **12**, 859 (1986).
- ²³P. García-Fernández, J. C. Wojdel, J. Íñiguez, and J. Junquera, Second-principles method for materials simulations including electron and lattice degrees of freedom, *Phys. Rev. B* **93**, 195137 (2016).
- ²⁴W. M. C. Foulkes and R. Haydock, Tight-binding models and density-functional theory, *Phys. Rev. B* **39**, 12520 (1989).
- ²⁵Z.-P. Cao, Y.-J. Zhao, J.-H. Liao, and X.-B. Yang, Gap maximum of graphene nanoflakes: a first-principles study combined with the monte carlo tree search method, *RSC Adv.* **7**, 37881 (2017).
- ²⁶A. Chandrasekaran, D. Kamal, R. Batra, C. Kim, L. Chen, and R. Ramprasad, Solving the electronic structure problem with machine learning, *Npj Comput. Mater.* **5**, 22 (2019).
- ²⁷P. B. Jørgensen and A. Bhowmik, Equivariant graph neural networks for fast electron density estimation of molecules, liquids, and solids, *Npj Comput. Mater.* **8**, 183 (2022).
- ²⁸B. G. del Rio, B. Phan, and R. Ramprasad, A deep learning framework to emulate density functional theory, *Npj Comput. Mater.* **9**, 158 (2023).
- ²⁹E. D. Glendening and F. Weinhold, Natural resonance theory: I. general formalism, *Journal of Computational Chemistry* **19**, 593 (1998).
- ³⁰M. H. Lee, Ergodic theory, infinite products, and long time behavior in hermitian models, *Phys. Rev. Lett.* **87**, 250601 (2001).
- ³¹E. Aghion, D. A. Kessler, and E. Barkai, From non-normalizable boltzmann-gibbs statistics to infinite-ergodic theory, *Phys. Rev. Lett.* **122**, 010601 (2019).
- ³²I. Langmuir, The octet theory of valence and its applications with special reference to organic nitrogen compounds, *J. Am. Chem. Soc.* **42**, 274 (1920).
- ³³S. Xu, C. He, Y. Zhao, X. Yang, and H. Xu, Generalized octet rule with fractional occupancies for boron, *J. Am. Chem. Soc.* **145**, 25003 (2023).
- ³⁴M. Solà, Forty years of Clar’s aromatic π -sextet rule, *Front. Chem.* **1**, 22 (2013).
- ³⁵A. Karton, How reliable is DFT in predicting relative energies of polycyclic aromatic hydrocarbon isomers? comparison of functionals from different rungs of jacob’s ladder, *J. Comput. Chem.* **38**, 370 (2017).
- ³⁶E. D. Glendening, C. R. Landis, and F. Weinhold, Resonance theory reboot, *J. Am. Chem. Soc.* **141**, 4156 (2019).
- ³⁷G. Kresse and J. Furthmüller, Efficient iterative schemes for *ab initio* total-energy calculations using a plane-wave basis set, *Phys. Rev. B* **54**, 11169 (1996).
- ³⁸G. Kresse and D. Joubert, From ultrasoft pseudopotentials to the projector augmented-wave method, *Phys. Rev. B* **59**, 1758 (1999).
- ³⁹J. Paier, M. Marsman, K. Hummer, G. Kresse, I. C. Gerber, and J. G. Ángyán, Screened hybrid density functionals applied to solids, *J. Chem. Phys.* **124**, 154709 (2006).
- ⁴⁰J. Heyd, G. E. Scuseria, and M. Ernzerhof, Hybrid functionals based on a screened Coulomb potential, *J. Chem. Phys.* **118**, 8207 (2003).
- ⁴¹H. Miyoshi, S. Nobusue, A. Shimizu, and Y. Tobe, Non-alternant non-benzenoid kekulenes: the birth of a new kekulene family, *Chem. Soc. Rev.* **44**, 6560 (2015).
- ⁴²J. C. Buttrick and B. T. King, Kekulenes, cycloarenes, and heterocycloarenes: addressing electronic structure and aromaticity

- through experiments and calculations, *Chem. Soc. Rev.* **46**, 7 (2017).
- ⁴³G. Povie, Y. Segawa, T. Nishihara, Y. Miyauchi, and K. Itami, Synthesis of a carbon nanobelt, *Science* **356**, 172 (2017).
- ⁴⁴C. C. Moore, Ergodic theorem, ergodic theory, and statistical mechanics, *Proc. Natl. Acad. Sci. U.S.A.* **112**, 1907 (2015).
- ⁴⁵J. S. Rowlinson, Probability, information and entropy, *Nature* **225**, 1196 (1970).
- ⁴⁶S. Chen, P. Slattum, C. Wang, and L. Zang, Self-assembly of perylene imide molecules into 1d nanostructures: Methods, morphologies, and applications, *Chem. Rev.* **115**, 11967 (2015).
- ⁴⁷W. Jiang and Z. Wang, Molecular carbon imides, *J. Am. Chem. Soc.* **144**, 14976 (2022).
- ⁴⁸L. Ma, Y. Han, Q. Shi, and H. Huang, The design, synthesis and application of rubicene based polycyclic aromatic hydrocarbons (pahs), *J. Mater. Chem. C* **11**, 16429 (2023).
- ⁴⁹Y. Ruiz-Morales, Homo-lumo gap as an index of molecular size and structure for polycyclic aromatic hydrocarbons (pahs) and asphaltenes: A theoretical study. i, *J. Phys. Chem. A* **106**, 11283 (2002).
- ⁵⁰Y. Ruiz-Morales, Application of the γ -rule and theoretical study to understand the topological and electronic structures of polycyclic aromatic hydrocarbons from atomic force microscopy images of soot, coal asphaltenes, and petroleum asphaltenes, *Energy Fuels* **36**, 8725 (2022).
- ⁵¹S. J. Cyvin, J. Brunvoll, and B. N. Cyvin, Enumeration and classification of coronoid hydrocarbons. 10. double coronoids, *J. Chem. Inf. Comput.* **30**, 210 (1990).
- ⁵²D. Malko, C. Neiss, F. Viñes, and A. Görling, Competition for graphene: Graphynes with direction-dependent Dirac cones, *Phys. Rev. Lett.* **108**, 086804 (2012).
- ⁵³B. G. Kim and H. J. Choi, Graphyne: Hexagonal network of carbon with versatile Dirac cones, *Phys. Rev. B* **86**, 115435 (2012).
- ⁵⁴S.-G. Xu, X.-T. Li, Z.-J. Chen, C.-C. He, C. He, X.-B. Yang, and H. Xu, Toward hidden materials with directional bonds, *Phys. Rev. Mater.* **7**, 084202 (2023).
- ⁵⁵Y. Hu, C. Wu, Q. Pan, Y. Jin, R. Lyu, V. Martinez, S. Huang, J. Wu, L. J. Wayment, N. A. Clark, M. B. Raschke, Y. Zhao, and W. Zhang, Synthesis of γ -graphyne using dynamic covalent chemistry, *Nat. Synth.* **1**, 449 (2022).